Article:
Alshehri, A., Baker, I.-M., English, D.M. et al. (2025) Mutations on the surface of HDAC1 reveal molecular determinants of specific complex assembly and their requirement for gene regulation. Nucleic Acids Research, 53 (17). gkaf918. ISSN: 0305-1048

https://doi.org/10.1093/nar/gkaf918

Nucleic Acids Research, 2025, **53**, gkaf918
https://doi.org/10.1093/nar/gkaf918
Molecular and Structural Biology

Mutations on the surface of HDAC1 reveal molecular determinants of specific complex assembly and their requirement for gene regulation

Ahmad Alshehri[1], India-May Baker[1], David M. English[1], Louise Fairall[2], Mark O. Collins[3], John W.R. Schwabe[2,*], Shaun M. Cowley[1,*]

[1]Department of Molecular and Cell Biology, University of Leicester, Leicester LE1 7RH, UK
[2]Leicester Institute for Structural and Chemical Biology and Department of Molecular and Cell Biology, University of Leicester, Leicester LE1 7RH, UK
[3]School of Biosciences, University of Sheffield, Sheffield S10 2TN, UK

[*]To whom correspondence should be addressed. Email: Smc57@le.ac.uk
Correspondence may also be addressed to John W.R. Schwabe. Email: js336@le.ac.uk

Abstract

Histone deacetylase 1 and 2 (HDAC1/2) regulate histone acetylation as catalytic and structural components of six unique multiprotein complex families: SIN3, NuRD, CoREST, MIDAC, MIER, and RERE. Co-immunoprecipitation of HDAC1-Flag followed by mass spectrometry revealed that 92% of HDAC1 in mouse embryonic stem cells resides in three complexes, NuRD (49%), CoREST (28%), and SIN3 (15%). We compared the structures of MTA1:HDAC1 and MIDEAS:HDAC1 to identify critical binding residues on the surface of HDAC1. Surprisingly, a single mutation, Y48E, disrupts binding to all complexes except SIN3. Rescue experiments performed with HDAC1–Y48E in HDAC1/2 double-knockout cells showed that retention of SIN3 binding alone is sufficient for cell viability. Gene expression and histone acetylation patterns were perturbed in both Y48E and a second mutant cell line, HDAC1–E63R, indicating that cells require a full repertoire of the HDAC1/2 complexes to regulate their transcriptome appropriately. Comparative analysis of MTA1/HDAC1 and SIN3B/HDAC2 structures confirmed the differential modes of HDAC1 recruitment, with Y48 interacting with ELM2/SANT domain-containing proteins, but not SIN3. The E63R mutation shows markedly reduced binding to NuRD and MiDAC complexes but retains some CoREST binding. We provide novel molecular insights into the abundance, co-factors and assemblies of this crucial family of chromatin modifying machines.

Graphical abstract

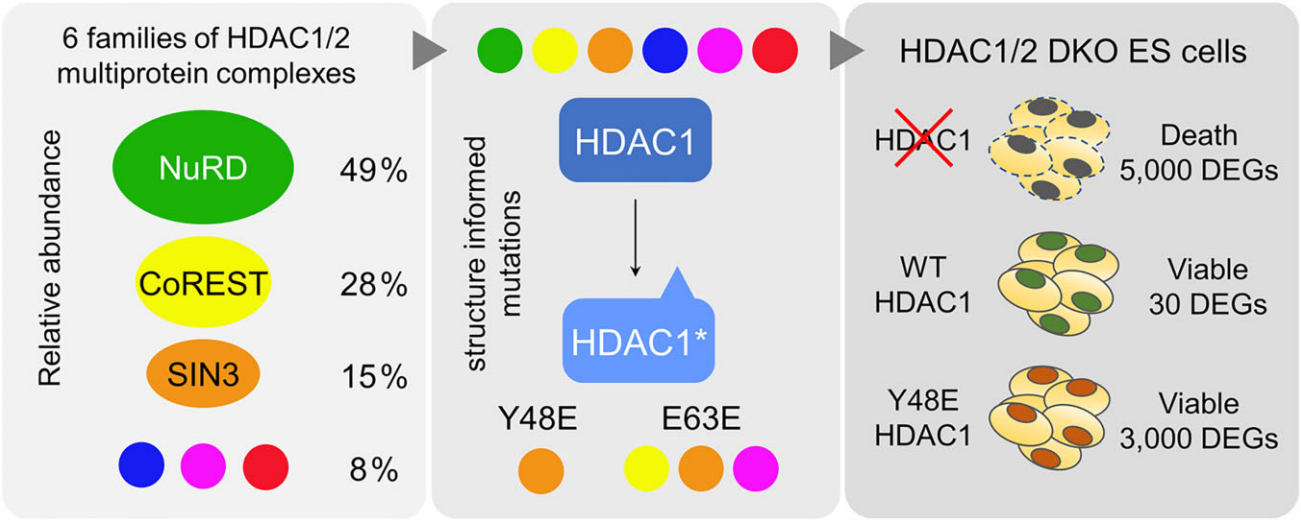

Introduction

The post-translational modification of histones is a fundamental mechanism for the regulation of chromatin organization in all eukaryotes. Acetylation of highly conserved lysines in the N-terminal tails of all four core histones leads to a loosening of chromatin structure as well as providing binding sites for acetyl-lysine reader proteins [1]. Critically, histone acetylation is a dynamic process, with a half-life of 30–120

Received: March 25, 2025. **Revised:** July 24, 2025. **Accepted:** August 20, 2025

min [2, 3], due to the interplay of histone acetyltransferase (HAT) and histone deacetylase (HDAC) enzymes. HDAC1 and HDAC2 (HDAC1/2) are highly conserved paralogues that serve as common catalytic components of six distinct families of multiprotein complex: SIN3, NuRD, CoREST, MiDAC, MIER and RERE. Each consists of a central platform (e.g. SIN3A) that mediates the binding of HDAC1/2 and numerous auxiliary proteins that add complementary activities [4, 5]. These include additional enzymatic activities, such as the helicase, CHD4 (NuRD), and lysine-specific demethylase 1 (LSD1/KDM1A) in CoREST. Within each family there are also distinct assemblies, SIN3A versus SIN3B for instance [6]. While retaining a similar domain structure, SIN3A and SIN3B form biochemically and structurally distinct complexes [7–15] resulting in different mouse knockout phenotypes [16–18]. An analogous arrangement also occurs in NuRD, where MTA1 interacts with either MBD2/3 or PWWP2A/B in a mutually exclusive manner to form discrete complexes with different functions [19]. A deeper understanding of the assembly and structure of these diverse complexes is essential to understanding the mechanism of HDAC1/2 activity in cells.

The 15 HDAC1-binding partners can be split into two main classes: the majority that employ ELM2–SANT domains (MTA1-3, RCOR1-3, MIER1-3, MIDEAS, TRERF1, ZNF541, and RERE) and the two highly related corepressors, SIN3A and SIN3B. With the exception of ZNF541 (testis-specific), the expression of these proteins is largely ubiquitous in human cells. Each cell type, therefore, has the option to employ 14 different HDAC1-binding platforms, with a multitude of accessory proteins, contributing both chromatin binding and modifying activities. In mice, knockout of critical components of the SIN3A, NuRD, CoREST, and MIDAC complexes results in embryonic lethality [16, 20–23], suggesting that each possesses a unique and essential function. Why cells contain such a variety of vehicles for HDAC1/2 activity remains to be fully understood. Structural biology has provided insights into the assembly of these macromolecular machines. In addition to a unique set of components, complexes have either monomeric (CoREST and SIN3B/Rpd3s), dimeric (SIN3A/Rpd3L and NURD), or tetrameric (MiDAC) assemblies [7–14, 21, 24, 25], particularly pertinent for nucleosomal substrates containing two copies of each core histone.

To disentangle unique from overlapping activities of HDAC1/2 complexes, we require additional information about complex components, their relative abundance and mode of assembly. For example, are all complex components present in the same amount? And if not, what constitutes a "core" complex? To address these questions, we have performed a quantitative mass spectrometry analysis of HDAC1/2 complexes purified from mouse embryonic stem cells (ESCs) and found that the majority of HDAC1 is present in just three complexes (NuRD, CoREST, and SIN3A), with a relatively small set of unique core components. Their assembly utilizes HDAC1 as an integral structural component, with conserved residues on the surface of the enzyme contributing to a highly stable association. Comparative structural analysis of individual ELM2–SANT domains bound to HDAC1 allowed the identification of key surface residues. Surprisingly, given an extensive protein–protein interaction surface, we found that single point mutations on the surface of HDAC1 were sufficient to perturb binding to its partners. Furthermore, by interrogating individual binding regions, we have identified the first mutations of their kind that allow us to discriminate between different HDAC1-binding proteins and their associated complexes. By probing how HDAC1/2 complexes are assembled, we have gained insights into their unique functions, and the first indications of how to perturb specific complexes inside cells.

Materials and methods

Cell culture

All experiments described in this research used *Hdac1/2*$^{lox/lox}$ ES cells cultured as described previously in M15 + leukaemia inhibitory factor (LIF) media [26]. These cells were engineered to stably express either wild-type (WT) HDAC1 rescue or HDAC1 mutants as indicated. To induce deletion of endogenous *Hdac1/2*, cells were cultured with 1 μM 4-hydroxytamoxifen (OHT) for 24 h and then cultured for a further 4 days to ensure complete removal of endogenous HDAC1/2 before use in the experiments detailed below.

Lipofectamine 2000 stable transfections

The cloning of all constructs used in this work was performed by the PROTEX service at the University of Leicester. Stable transfection was achieved by co-transfecting Hdac1/2$^{lox/lox}$ cells with *piggyBac* transposase and expression vectors as described previously [27].

CellTiter-Glo assays

For each HDAC1 mutant, 500 cells were seeded per well in triplicate on 96-well plates (−/+ OHT). Five days later CellTiter-Glo (CTG) assays (Promega) were conducted as per the manufacturer's instructions.

Crystal Violet viability assays

For each HDAC1 mutant, 8 × 10^5 cells were seeded into six-well plates in triplicate (−/+ OHT). Five days post OHT treatment media was removed and cells were washed once with PBS prior to fixing with 1 ml of 100% methanol for 2 min. Methanol was removed and cells were washed once with PBS before being left to dry for 3 h at room temperature. One milliliters of Crystal Violet reagent (ProLab; PL.7000) was then added to each well for 2 min, then cells were washed with water. Plates were allowed to dry for 24 h before imaging.

Co-immunoprecipitations

Five days prior to the co-immunoprecipitations (coIPs), HDAC1 rescue cell lines were treated with 1 μM OHT to remove endogenous HDAC1/2. Cell pellets from a confluent 10-cm plate were lysed in an appropriate volume of coIP buffer [250 mM NaCl, 20 mM Tris–HCl pH 7.5, 0.5% IGEPAL, 1 mM EDTA, and Protease inhibitor (Roche, 05892791001)] on ice for 30 min. Lysed samples were then centrifuged at 14 000 rpm at 4°C for 15 min; the supernatant containing the protein extract was retained, and the concentration was determined by Bradford assay. Extracts were diluted to a concentration of 5 μg/μl using coIP buffer and 300 μl was used per IP. Sixty microliters of Protein G Dynabeads (Thermo Fisher; 10003D) was washed three times with coIP buffer and then resuspended in an equal volume of coIP buffer to the original volume of bead slurry before the addition of 1 μg of Flag or normal mouse IgG antibodies. Antibodies were bound to beads via rotation at 4°C for 1 h. Beads were again washed

in 500 µl of coIP buffer and then resuspended in 200 µl of coIP buffer before being split equally between IPs. IPs were incubated at 4°C overnight (18 h) with rotation, and 20% of the protein extract was kept as an input before the addition of beads. IPs were then washed three times with coIP buffer before being used for western blotting or mass spectrometry as described below.

Western blotting

Western blots were performed as described previously [26]. Where coIP samples were used for western blotting, the beads were resuspended in 100 µl of coIP buffer before the addition of 4× loading buffer (Invitrogen; NP0007) and denaturation at 95°C for 5 min.

Preparation of HDAC1-Flag pulldown samples for mass spectrometry analysis

HDAC1-Flag pulldown samples were eluted by heating in 5% SDS, 50 mM Tris pH 7.4 at 70°C for 20 min; triethylammonium bicarbonate (TEAB) was then added to a final concentration of 50 mM with a pH of 8. Tris(2-carboxyethyl) phosphine hydrochloride (TCEP) was added to a final concentration of 5 mM, and samples were heated to 70°C for 15 min. Iodoacetamide (IAA) was then added to a final concentration of 10 mM, and samples were incubated at 37°C in the dark for 30 min. Samples were acidified with 4 µl of 12% phosphoric acid, and 264 µl of S-Trap-binding buffer (90% methanol, 100 mM TEAB pH 7.1) was then added to each sample. Samples were then passed through S-Trap columns 150 µl at a time by centrifugation at 4000 rpm for 30 s. Samples were washed four times with 150 µl of S-Trap-binding buffer through centrifugation at 4000 rpm for 30 s. Two micrograms of trypsin (Pierce, sequencing grade) was added to each sample, and digestion was allowed to proceed at 47°C for 80 min. Peptides were eluted with 40 µl of 50 mM TEAB, 40 µl of 0.2% aqueous formic acid, and 40 µl of 50% acetonitrile with 0.2% formic acid, with centrifugation at 4000 rpm for 30 s for each elution. Eluted peptides were dried in a vacuum concentrator and resuspended in 0.5% formic acid for LC-MS/MS analysis.

Preparation of histone samples for mass spectrometry analysis

To obtain histone proteins a whole cell extract was first made by lysing cell pellets from confluent 10-cm plates in NP-40 lysis buffer [50 mM Tris–HCl pH 8, 150 mM NaCl, 1 mM EDTA, 1% NP-40, 10% glycerol, and protease inhibitor cocktail (Sigma, P8340)] for 30 min. Lysates were cleared by centrifugation at 14 000 rpm at 4°C for 15 min. The supernatant containing the whole cell extract was transferred to a fresh tube and histones were extracted from the remaining pellet by overnight incubation (20 h) in 50 µl of 0.4 N H_2SO_4. Samples were again centrifuged at 14 000 rpm at 4°C for 15 min, and the supernatant containing the histone proteins was transferred to a fresh tube. The samples were then neutralised using 0.8 N NaOH. Histones were derivatized according to [28]. Briefly, 10 µg of histone samples in 50 µl of 50 mM ammonium bicarbonate were incubated with 16.6 µl of propionylation reagent (1:3 v/v propionic anhydride in acetonitrile) for 15 min at 37°C with shaking at 900 rpm. Samples were dried down in a vacuum concentrator and the derivatization steps were repeated. Ten micrograms of derivatized histone samples were digested with 1 µg of trypsin in 50 µl of 50 mM ammonium bicarbonate for 2 h at 37°C with shaking at 900 rpm. Digests were desalted using C18 spin columns (Thermo Fisher, 89870) according to the manufacturer's protocol. Eluted peptides were dried in a vacuum concentrator and resuspended in 0.5% formic acid for LC-MS/MS analysis.

Mass spectrometry analysis

Each sample was analysed using nanoflow LC-MS/MS using an Orbitrap Elite (Thermo Fisher) hybrid mass spectrometer equipped with an EasySpray source, coupled to an Ultimate RSLCnano LC System (Dionex). Peptides were desalted online using a nano-trap column, 75 µm I.D.X 20 mm (Thermo Fisher) and then separated using a 120-min gradient from 5% to 35% buffer B (0.5% formic acid in 80% acetonitrile) on an EASY-Spray column, 50 cm × 50 µm ID, PepMap C18, 2 µm particles, 100 Å pore size (Thermo Fisher). The Orbitrap Elite was operated in Data-Dependent Acquisition (DDA) mode with a cycle of one MS (in the Orbitrap) acquired at a resolution of 120 000 at m/z 400, a scan range 375–1600, with the top 20 most abundant multiply charged (2 + and higher) ions in a given chromatographic window subjected to MS/MS fragmentation in the linear ion trap using CID. A Fourier Transform Mass Spectrometry (FTMS) target value of 1e6 and an ion trap MSn target value of 1e4 were used with the lock mass (445.120025) enabled. Maximum FTMS scan accumulation time of 200 ms and maximum ion trap MSn scan accumulation time of 50 ms were used. Dynamic exclusion was enabled with a repeat duration of 45 s with an exclusion list of 500 and an exclusion duration of 30 s.

Mass spectrometry data analysis

Raw mass spectrometry data were analysed using MaxQuant version 1.6.10.43. The following parameters were used to search against a mouse reference proteome: digestion set to Trypsin/P with three missed cleavages, methionine oxidation, N-terminal protein acetylation, and lysine acetylation set as the variable modifications. Additionally, propionylation was set as a variable modification for derivatized histone samples with the number of missed cleavages set to 5. A protein and peptide false discovery rate (FDR) of 0.01 were used for identification level cut-offs based on a decoy searching database strategy. Protein group output files generated by MaxQuant were loaded into Perseus version 1.6.10.50. The matrix was filtered to remove all proteins that were potential contaminants, only identified by site and reverse sequences. The LFQ intensities were then transformed by log2(x), normalized by subtraction of the median value, and individual intensity columns were grouped by experiment. Proteins were filtered to keep only those with a minimum of three valid values in at least one group. The distribution of intensities was checked to ensure standard distribution for each replicate. Missing values were randomly imputed with a width of 0.3 and downshift of 1.8 from the standard deviation. To identify significant differences between groups, two-sided Student's t-tests were performed with a permutation-based FDR of 0.05. The mass spectrometry data have been deposited to the ProteomeXchange Consortium via the PRIDE partner repository with the dataset identifiers [PXD060154 (HDAC1 pulldowns) and PXD060158 (histone analysis)].

Deacetylase assays

In vitro HDAC assays were conducted on whole cell extracts made from cells expressing the different HDAC1 mutants extracted in HDAC assay buffer containing 50 mM NaCl, 50 mM Tris–HCl pH 7.5, 5% glycerol, 0.3% Triton X-100 using a Boc-Lys(Ac)-AMC substrate as described previously [26]. One-way ANOVA multiple hypothesis testing was performed using GraphPad Prism to determine significant changes in deacetylase activity ($n = 3$).

RNA-sequencing

RNA was extracted from cell pellets collected from a 6 cm plate using the TRI Reagent (Zymo Research, R2050-1-200) based Direct-Zol RNA MiniPrep Kit (Zymo Research, R2052) following the manufacturer's instructions. RNA quality was determined by the NUCLEUS facility at the University of Leicester using an Agilent RNA 6000 Nano Chip on an Agilent 2100 Bioanalyzer. Library preparation and sequencing was carried out by Novogene, and samples were sequenced to a depth of 20 million reads on the Illumina NovaSeq 6000 PE150 sequencing platform. Bioinformatic analysis was performed as described in [29] with reads mapped to the mm10 genome index. The processed files can be found at the Gene Expression Omnibus (GEO), series GSE278462. For gene ontology (GO) analysis, the Bioconductor package TopGO [30] was used with the mouse genome-wide annotation package org.Mm.eg.db.

Results

NuRD, CoREST, and SIN3A are the dominant HDAC1/2 complexes in cells

To examine the composition and stoichiometry of HDAC1/2 containing complexes, we stably expressed HDAC1 with a C-terminal Flag tag in conditional *Hdac1/2* double knockout (DKO) ESCs (Fig. 1A). Treatment with 4-hydroxytamoxifen (OHT) activates removal of the endogenous HDAC1/2 proteins within 4 days causing a complete loss of cell viability [26]. Introduction of HDAC1-flag rescues viability, confirming its functionality, which allows us to assess HDAC1-associated proteins using coIP and mass spectrometry (Fig. 1B). We identified 148 proteins significantly enriched in the pulldown, compared to DKO cells lacking HDAC1-Flag as a control (Supplementary Table S1). Components of all six HDAC1/2 complexes were present among this list. To estimate the abundance of individual proteins, we calculated intensity-based absolute quantification (iBAQ, [31]) values and manually curated proteins into SIN3A/B, NuRD, CoREST, MiDAC, MIER, and RERE complexes (Fig. 1B and C). Of the 14 HDAC1 interacting proteins expressed in ESCs, we detected 13 (Fig. 1B), with only RCOR3 absent, most probably due to lower expression levels. Using the iBAQ value for direct-HDAC1 binding proteins in each complex we estimated the relative abundance of the six complexes (Fig. 1B, indicated by red arrows). Almost half of the HDAC1 in ESCs was incorporated into the NuRD complex (49%), with CoREST (28%) and SIN3 (15%) being the next most abundant. Collectively, these three complexes make up the majority of HDAC1 complexes in the cell at 92%. MIER (4%), MiDAC (3%), and RERE1 (1%) are minor species in ESCs, albeit, in the case of MiDAC, still essential for development [21]. Reassuringly, the sum-total iBAQ value of HDAC1-binding proteins is 91% of the total HDAC1-Flag recovered in the pulldown, consistent with the 1:1 interaction between HDAC1 and its binding partners observed in multiple structural determinations [21, 24, 25]. The estimated relative stoichiometry of individual complex components allowed a number of compelling insights. For example, the SIN3A complex and its core components (SIN3A, SUDS3, and SAP30) appear to be at least 10-fold more abundant in ESCs than the SIN3B complex (SIN3B, EMSY, and ARID4B). The NuRD complex incorporates either methyl-CpG-binding domain protein 2 (MBD2) or MBD3 in a mutually exclusive manner [32]. Here, we show that MBD3 is clearly the major constituent in ESCs with a 10:1 MBD3/MBD2 ratio. Stoichiometric components of NuRD (based on MTA1-3 and MBD3 levels) include CHD4, GATA2A, and GATA2B; while ZNF219, PARP1, and the helicase, CHD3 are only minor constituents. The core of CoREST consists of LSD1, RCOR1 or RCOR2, and HDAC1, with smaller amounts of ZMYM2. Notable CoREST-associated proteins, CTBP1 and CTBP2, appear to be sub-stoichiometric members of the complex. MIDEAS and TRERF1 are both ELM2–SANT-containing proteins that are likely interchangeable HDAC1-binders within MiDAC, with the former being the dominant component in ESCs. Both proteins interact with DNTTIP1, which was present in our ESC extracts, but did not reach significance following coIP (Supplementary Table S1). RBBP4 and RBBP7 are well-known histone-binding subunits of multiple chromatin-modifying machines, including SIN3A, NuRD, and PRC2 [33–37]. We observed abundant levels of both proteins associated with HDAC1 and the RBBP4/RBBP7 ratio was 10:1 in our experiments (Fig. 1D). Intriguingly, we measured almost twice as much RBBP4 as HDAC1, consistent with a 2:1:1 ratio of RBBP4/MTA1/HDAC1 in NuRD [32]. Numerous HDAC1-associated transcription factors were also identified, most notably, SALL4, which is required for ESC pluripotency and is known to bind NuRD [38–40]. Most of the other transcription factors identified were purified at levels far below those of the core complex components, which reflect both their relative expression levels and the transient nature of their association. We also observed a number of chromatin-modifying enzymes, including TET1 and O-GlcNAc transferase (OGT), known to bind to the SIN3A complex [41, 42] and both EHMT1 (KMT1D/GLP) and EHMT2 (KMT1C/G9A), euchromatic histone H3 Lys9 methyltransferases, with roles in gene silencing.

ELM2/SANT and SIN3 proteins utilize distinct interacting surfaces on HDAC1

13 of 15 HDAC1-binding proteins utilize adjacent ELM2–SANT domains to directly interact with HDAC1 [4, 5]. The schematic diagram in Fig. 2A (left) shows the effective arrangement of these two domains across the surface of HDAC1, based on high-resolution structures of MTA1:HDAC1 and MIDEAS:HDAC1 (Fig. 2A, right) [21, 24]. The SANT domain consists of three α-helices, which together with a positively charged surface on HDAC1, sandwiches a molecule of inositol phosphate (InsP) necessary for full enzymatic activity [43]. The ELM2 domain has a bipartite structure, with an unstructured N-terminal region that lies across a highly conserved groove on the underside of HDAC1, and a C-terminal region containing a three α-helical bundle that sits adjacent to the SANT domain. These extensive interactions can be subdivided into three discrete re-

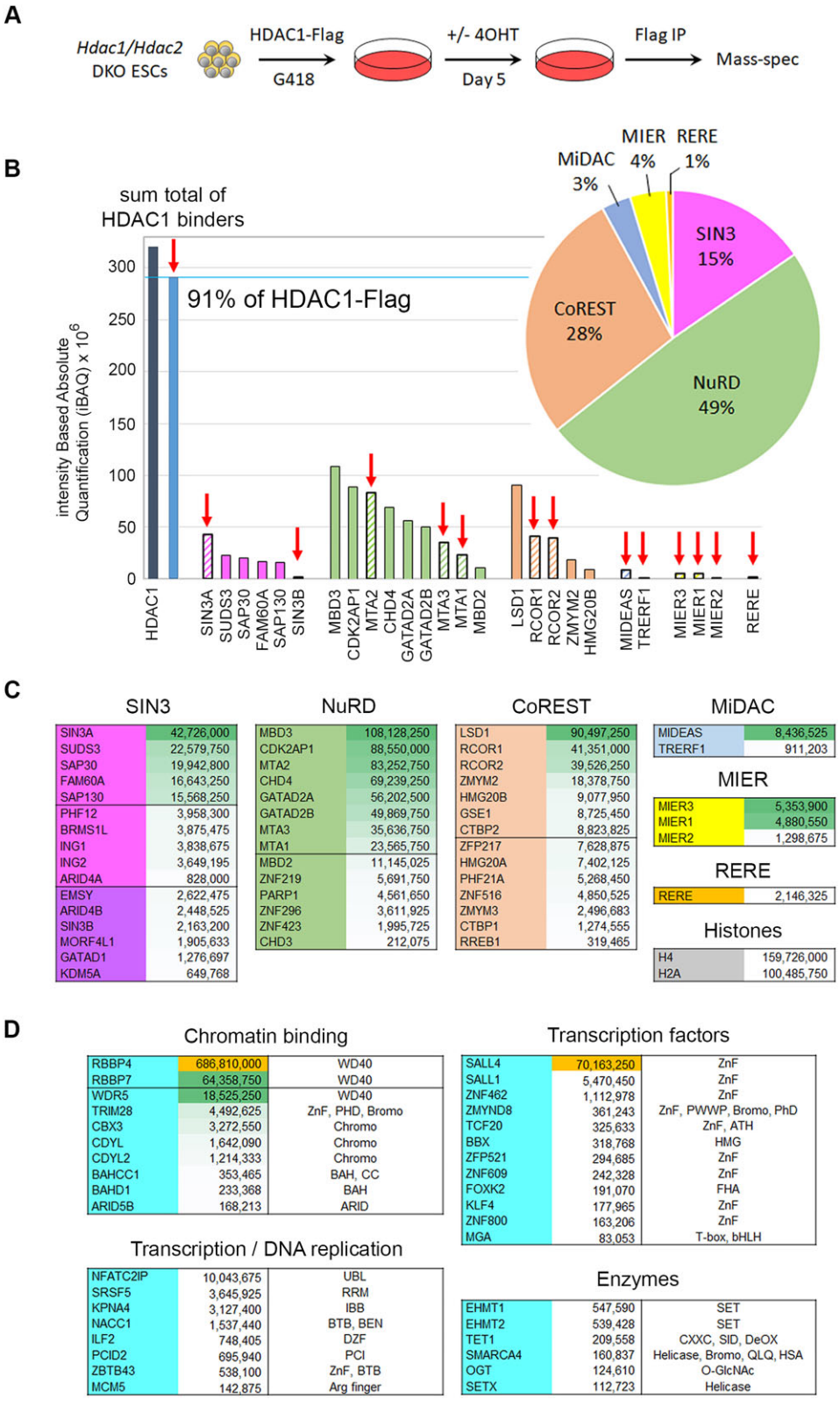

Figure 1 Relative abundance of HDAC1-binding proteins and associated complex components. (**A**) Schematic showing experimental procedure to produce HDAC1-Flag coIP mass spectrometry in *Hdac1/2* DKO cells. (**B**) Graph shows iBAQ values for core components of the six unique HDAC1/2 complexes as indicated. The red arrow indicates proteins that directly bind to HDAC1. The pie chart indicates the relative proportion of the six HDAC1/2 complexes determined by the iBAQ values for direct HDAC1-binding components from each complex. (**C**) Table showing the iBAQ values for components of the indicated HDAC1/2 complexes ranked in order of abundance. (**D**) Table shows iBAQ values for significantly enriched HDAC1-associated proteins grouped into the indicated functional groups. Domains contained by these proteins are also indicated.

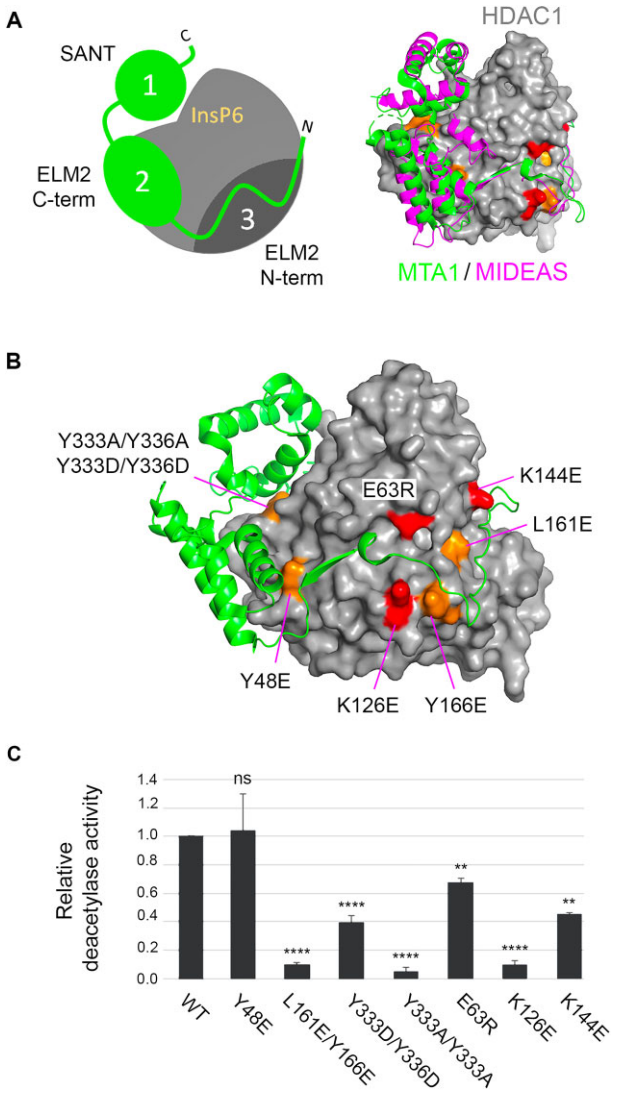

Figure 2 Defining critical interactions on the surface of HDAC1. (**A**) Left panel: a schematic diagram outlining three separate regions used by ELM–SANT domain-containing HDAC1-binding proteins. The right panel shows an overlay of MTA1/HDAC1 and MIDEAS/HDAC1 binary complexes, showing a conserved mechanism of HDAC1 binding. (**B**) HDAC1/MTA1 binary showing the position of individual residues mutated in the study. Orange, aromatic/non-charged residues; red, charged residues. (**C**) The deacetylase assay was performed using enzymes co-immunoprecipitated from HEK293T cell transfected with either WT HDAC1 or the indicated mutants. A one-way ANOVA was performed compared to WT values. NS, not significant, $P > 0.05$, ** ≤ 0.01, **** ≤ 0.0001.

gions (Fig. 2A, see left panel): SANT (1), ELM2-C (2), and ELM2-N (3). To identify residues on the surface of HDAC1 required for interaction with the six unique multiprotein complexes, we used the MTA1/HDAC1 structure to design mutations in regions 1, 2, and 3 to perturb binding. In region 1, we focused on a pair of Tyr residues, Y333/Y336 (Fig. 2B), that mediate interactions with phosphates of the InsP6 and residues in α3 of the SANT domain. We mutated Y48 in region 2 which forms interactions with α2 of the ELM2-C domain. Region 3 forms an extended surface over which the unstructured ELM2-N domain stretches, forming a variety of interactions (Fig. 2B). We, therefore, chose three charged (E63R, K126E, and K144E), one hydrophobic (L161E), and one aromatic/non-polar (Y166E) mutations that span both the breadth and diversity of this region. Initially, we tested the effects of these mutations on HDAC1 when expressed and purified from HEK293T cells (Supplementary Fig. S1). HDAC1 expression levels were unaffected by the mutations; however, we observed significant changes in their relative deacetylase activity. HDAC1 Y333A/Y336A, K126E, and L161E/Y166R all showed activity below 10% of WT. Since none of these residues are adjacent to the active site, we infer residues on the surface of HDAC1 interacting with both SANT (region 1) and ELM2-N (region 3) contribute indirectly to enzymatic activity. In contrast, HDAC1 Y48E and E63R showed activity close to that of the WT enzyme. To monitor the interaction of WT and mutant HDAC1 with SIN3A we expressed both proteins transiently and performed a Flag-coIP, followed by western blotting. Intriguingly, we found a robust interaction between exogenous HDAC1-Flag and Myc-SIN3A proteins, but not endogenous SIN3A (Supplementary Fig. S1, compare red and green bands in the input versus coIP), suggesting that there is little interchange between corepressor and HDAC1 once the complex is assembled in cells. Mutation of Y333/Y336 to Ala or Asp reduced binding to all complexes, demonstrating the necessity of residues within region 1. In contrast, Y48E in region 2, bound to SIN3A while abolishing any interaction with RCOR1 (Supplementary Fig. S1—middle and lower panels). Thus, demonstrating for the first time, distinct surface requirements between HDAC1-binding proteins.

To examine the HDAC1 mutants in a more physiological environment, we used the piggyBAC system to stably introduce them into *Hdac1/2* DKO ESCs, so that following removal of the endogenous proteins (5 days post OHT), we could assess their capacity to rescue cell viability and interact with all six families of multiprotein complexes (Fig. 3A). We examined the survival of DKO cells expressing either WT or mutant HDAC1 using Crystal Violet staining (Fig. 3B) and CellTiter-Glo (Fig. 3C). Both assays revealed that expression of WT HDAC1 and E63R recovered cell viability to control levels, while Y333A/Y336A, K126E, and L161E/Y166E (which all displayed severely reduced HDAC activity) were incapable of rescuing the cell death phenotype. Intriguingly, cells expressing HDAC1–Y48E, which only bound SIN3A in HEK293T experiments, showed ∼50% cell viability in DKO ESCs, suggesting that retention of SIN3A binding alone is sufficient to retain some level of cell viability. Since HDAC1–Y48E and E63R mutants produced viable cells, we took these forward and performed large-scale coIPs for western blotting (Fig. 3D) and mass spectrometry (Fig. 3E) using DKO cells lacking a Flag epitope as a control ($n = 4$). WT HDAC1-Flag pulled down endogenous SIN3A, LSD1, MTA1, and DNTTP1 from ESCs, thus showing incorporation into the SIN3, CoREST, NuRD, and MiDAC complexes respectively (Fig. 3D). In contrast, the Y48E mutation bound only to SIN3A, while disrupting binding to all ELM2–SANT-containing partners (LSD1, MTA1, and DNTTIP1). HDAC1–E63R bound SIN3A and LSD1, but not MTA1 or DNTTIP1, thus demonstrating the ability to differentiate between individual ELM2–SANT-containing complexes.

To extend this analysis to all complexes and their components, we used material from the Flag-coIP to identify proteins bound to WT HDAC1, Y48E, and E63R via mass spectrometry (Fig. 3E). We performed statistical analysis (Student's *t*-test permutation-based FDR 0.05, WT versus mutant) to evaluate changes in the binding of core components from all

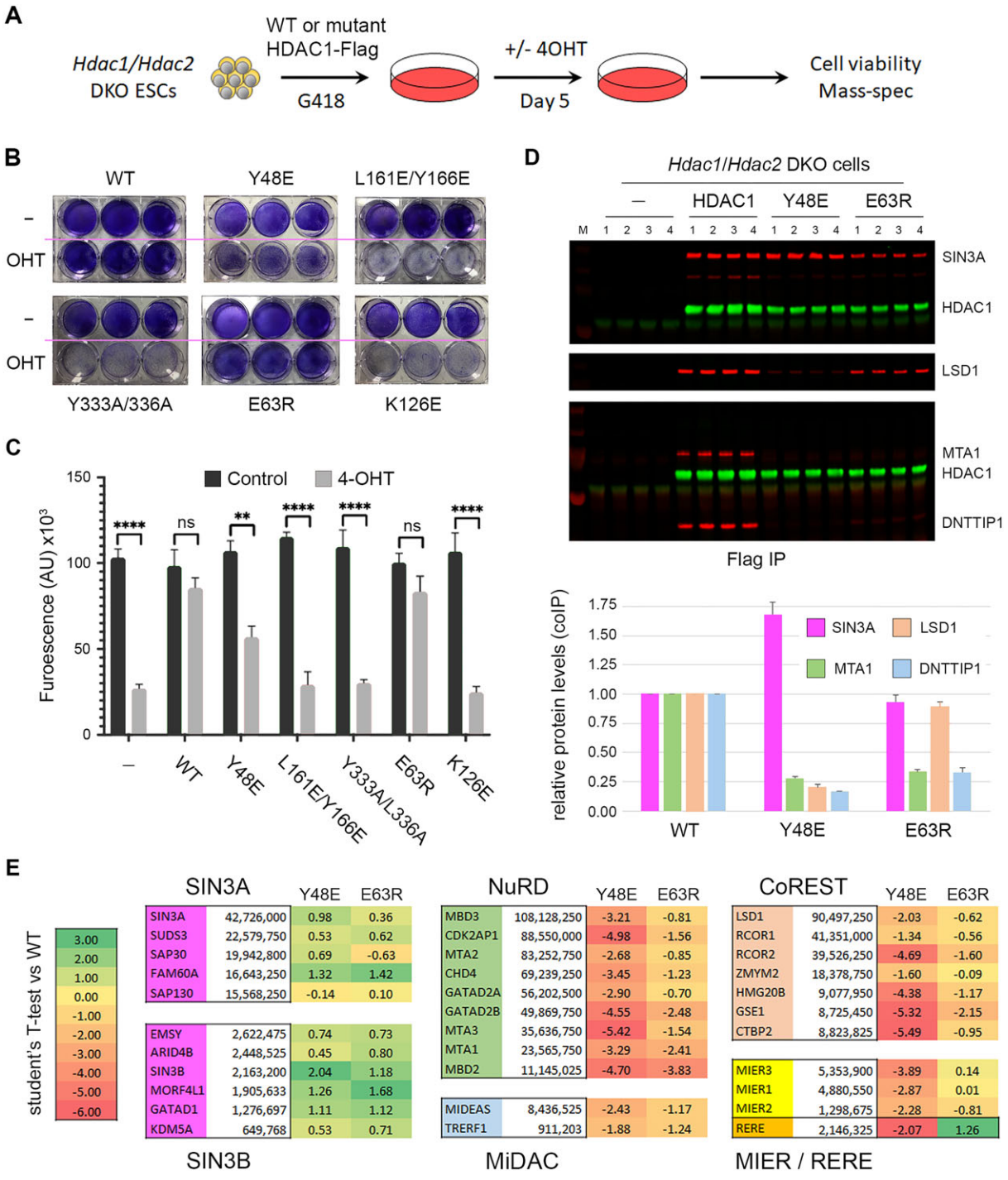

Figure 3 Individual point mutations discriminate between HDAC1-binding proteins. (**A**) Schematic showing experimental procedure to reintroduce HDAC1-Flag, or the indicated mutants to *Hdac1/2* DKO cells for cell viability and coIP/mass spectrometry experiments. The ability of WT and mutant HDAC1 to rescue the viability of HDAC1/2 DKO cells using (**B**) Crystal Violet staining of cells at 5 days post OHT treatment, and (**C**) a CTG assay. A student's t-test of control versus knockout cell viability was performed for the indicated mutants; ** $P < 0.01$, *** $P < 0.001$ and **** $P < 0.0001$ (**D**) Top panel, western blot for the indicated proteins following Flag-IP from DKO cells expressing either WT or Y48 and E63R mutations. Lower panel, quantification of the indicated proteins from western blot data normalized to the amount of HDAC1 in the coIP. Mean values for biological replicates ($n = 4$) are plotted with error bars indicating standard deviation from the mean. (**E**) The relative interaction of individual HDAC1/2 complex components was determined for Y48E and E64R mutants using mass spectrometry from $n = 4$ biological replicates. Values indicate $\log_2$ Student's *t*-test of the indicated mutant versus binding to WT HDAC1. Positive values show increased binding and negative values a relative reduction in binding compared to control.

HDAC1/2 containing multiprotein complexes to either Y48E or E63R. HDAC1–Y48E showed increased binding to all but one component of the SIN3A and SIN3B complexes (10 out of 11), but a strong reduction to all components of ELM–SANT-dependent complexes (22 out of 22). Thus, mutation of a single residue on the surface of HDAC1 in region 2 can abolish binding to 5 of 6 HDAC1/2 complex families. HDAC1–E63R also showed increased binding to SIN3A/B complexes and could further distinguish between ELM–SANT complexes. MIER1 and MIER3 showed no change in binding between WT and E63R, while RERE binding was slightly increased. In contrast, we observed reduced binding to all components of the NuRD and MiDAC complexes consistent with the absence of DNTTIP1 in western blots (Fig. 3D). We have thus identified two separate regions on the surface of HDAC1 capable of distinguishing incorporation into specific complexes. Y48E presents a black-and-white view of binding with disruption of all ELM2/SANT partners, retaining only SIN3A/B. HDAC1–E63R on the other hand, retains SIN3A/B, MIER1, RERE, and residual binding to CoREST, while abolishing the association of NuRD and MiDAC.

Retaining only a subset of HDAC1/2 complexes leads to histone hyperacetylation and loss of transcriptional regulation

HDAC1–Y48E and E63R retain HDAC activity (Fig. 2C) and the ability to rescue DKO ESC viability (Fig. 3B and C), but only bind to a limited number of HDAC1-interacting partners (Fig. 3D and E). Since only a subset of HDAC1/2 complexes remain active in these cells we hypothesized that this would cause changes in both histone acetylation and gene regulation. To examine this, we isolated histone proteins from control and HDAC1 mutant cells and then measured changes in acetylation levels by mass spectrometry (Supplementary Table S3). HDAC1–Y48E, which only binds SIN3A/B, caused significant increases in acetylation at multiple lysine residues within H2B, H3, and H4 compared to WT controls (Fig. 4A). Specific sites in H2B (K12, K15, and K20) and H3 (K14, K18, and K23) showed the greatest increase in acetylation. Interestingly, these same sites are also sensitive to loss of p300/CBP activity [2], suggesting an interplay of HDAC1/2 complexes with these critical HAT enzymes. HDAC1–E63R, which retains binding to SIN3A/B, CoREST, MIER, and RERE, and is therefore the weaker of the two mutants tested, showed more subtle changes in histone acetylation. Although we could detect increases in acetylation of H2B and H3 these did not reach statistical significance. Overall, this is consistent with E63R being incorporated into more HDAC1/2 complexes compared to Y48E.

We next examined the transcriptome of *Hdac1/2* DKO ESCs rescued with either HDAC1-WT or Y48E and E63R mutants (Fig. 4B). The addition of HDAC1-WT to DKO cells completely rescues the gene expression phenotype, with only minor changes in transcription (21 genes up and 8 down). In contrast, HDAC1–E63R produced significant numbers of differentially expressed genes (DEGs, 1001 up and 226 down). Consistent with its stronger effect on binding, the Y48E mutation produced a greater number of DEGs (2164 up and 987 down) (see Supplementary Table S2 for a complete list of DEGs). There is a clear correlation between the number of functional HDAC1/2 complexes and the number of dysregulated genes. We observed a significant overlap of genes between the two mutants, with 76% of DEGs in the E63R mutant coinciding with Y48E (Fig. 4C, 938 of 1227). GO analysis of overlapping DEGs from Y48E and E63R mutants identified significant changes in multiple pathways, including, placental development, vasculogenesis, and keratinization (Supplementary Fig. S2). A number of keratin genes showed significant de-repression, including *Krt5* (31-fold), *Krt14* (26-fold), *Krtdap* (9-fold), and *Krt8* (3-fold). Although we observed a good overlap between the two mutants, the majority of DEGs in Y48E cells were unique to that mutation (70%, 2201 of 3151). Among the pathways perturbed by HDAC1–Y48E was the cellular response to LIF, a critical signalling pathway for the maintenance of pluripotency in mouse ESCs. Upon closer examination, we observed down-regulation of multiple pluripotency-associated transcription factors, including, *Pou5f1*, *Nanog*, and *Esrrb* (Fig. 4D). ESCs have relatively low levels of DNA methylation, in part due to the repression of DNA methyltransferase (DNMT) enzymes by PRDM14 [44, 45]. The HDAC1–Y48E cells showed a decrease in PRDM14, consistent with a loss of pluripotency, and a corresponding increase in *Dnmt3a*, *Dnmt3b,* and *Dnmt3l* levels. These data demonstrate the requirement for a complete array of HDAC1/2 complexes for normal transcriptional regulation and homeostasis in ESCs.

Comparative analysis of HDAC1 binding partners reveals distinct interactions with a conserved interaction surface

To better understand the binding properties of Y48E and E63R mutants and the molecular determinants of HDAC1 interaction more generally, we performed a comparative analysis using binding partners from all six complex families. These include a recent cryoEM structure of SIN3B/HDAC2 [10], NuRD [12] and MiDAC [21, 32] complexes, as well as AlphaFold3 [46] models of MIER1 and RERE bound to HDAC1. What is immediately obvious, is that the mechanism of HDAC recruitment into the SIN3B complex is profoundly different to those complexes employing ELM2/SANT domains (Fig. 5A). SIN3B binding is largely confined to the surface of HDAC1 in proximity to the active site, opposite to Y48 and E63, explaining why these mutations have little effect on SIN3 binding (compare front versus back of HDAC1, Supplementary Fig. S3). In contrast, the ELM2–SANT domain is in direct contact with Y48. A conserved acidic residue is incompatible with the Y48E mutation. There are however binding surfaces conserved between SIN3 and ELM2–SANT binders, including Y333/Y336 (Fig. 5A), such that double mutation to Ala or Asp prevents both types of interaction (Supplementary Fig. S1). The HDAC surface around E63 provides an area of distinctiveness between ELM2–SANT binding partners. We found that MIER1 and RERE were unaffected or showed a slight increase in binding to the E63R mutation, respectively. Interaction with RCOR1 and RCOR2 from the CoREST complex was reduced, but western blotting clearly shows a residual interaction (Fig. 3D). All components NuRD and MiDAC were reduced (Fig. 3E). Examining the molecular details of these interactions, we identified conserved Arg (R189 in MTA1 and R130 in RCOR1) and Lys (K748 in MIDEAS) residues positioned directly towards E63, explaining why these three complexes are most affected by this mutation (Fig. 5B and C). The unstructured ELM2-N loop of RERE appears to circumvent E63 altogether, which explains

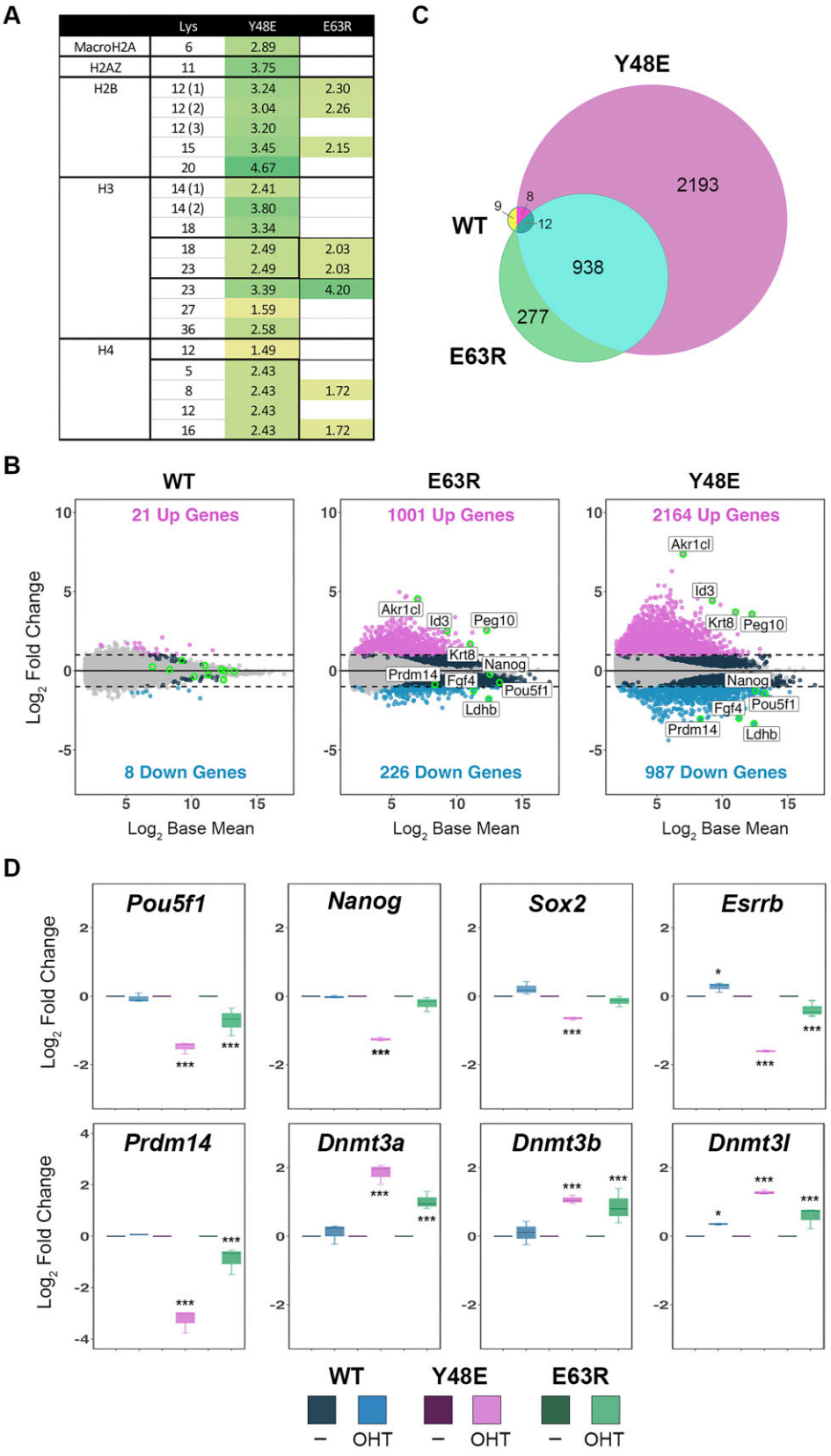

Figure 4 HDAC1 mutants that disrupt complex incorporation cause histone hyperacetylation and transcriptional dysregulation. (**A**) Change in acetylation relative to WT is shown for the indicated Lys residues, determined by mass spectrometry from $n = 4$ biological replicates. Brackets indicate measurements from unique peptides. Bold lines show multiple acetylation sites from the same peptide. Values are $\log_2$ Student's *t*-test values for each mutant versus WT controls. (**B**) MA plots indicate DEGs for *Hdac1/2* DKO cells rescued with WT or E63R and Y48E mutants from $n = 3$ biological replicates. Cut-offs applied were >2-fold change in expression, *P*-adjusted value < 0.01. (**C**) Venn diagram showing the number and overlap of DEGs from WT-, E63R-, and Y48E-expressing cells. (**D**) Boxplots displaying relative fold-change for the indicated genes. The adjusted *P*-values were taken from DESeq2 using a Wald test and the Benjamini and Hochberg method to correct for multiple hypothesis testing; * $P < 0.01$, *** $P < 0.0001$.

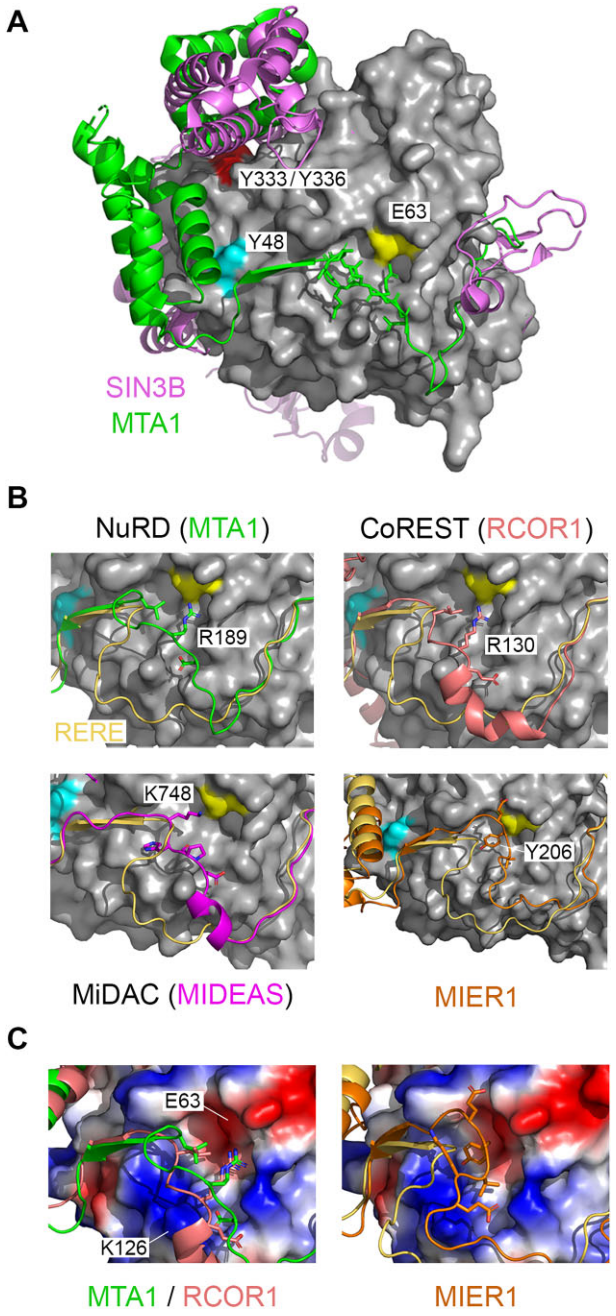

Figure 5 HDAC1-binding proteins have distinct modes of interaction. (**A**) Binary structures of MTA/HDAC1 (5ICN) and SIN3B/HDAC2 (8BPA) are superimposed to demonstrate different binding modalities. Residues required for interaction with binding partners are labelled. (**B**) A binding pocket centred on HDAC1–E63 (yellow) displays conserved and distinct interactions with ELM2/SANT-containing partners as indicated. An AlphaFold3 model of HDAC1/RERE (gold) is used as a reference point for other ELM2/SANT interactors. Panel (**C**) shows the electrostatic surface around HDAC1–E63 utilized by MTA1 and RCOR1, in contrast to MIER1.

the increased binding to the E63R mutant (Fig. 3E), particularly in the absence of competing HDAC1 binders. MIER1 associates with the HDAC1–E63 pocket using a non-polar interaction with Y206 and is thus unaffected by the switch in charge (Fig. 5C). By exploiting the unexpected sensitivity of HDAC1-binding proteins to specific surface residues, we are now able to differentiate between the recruitment of these crucial histone-modifying machines.

Discussion

The majority of histone-modifying enzymes operate in multiprotein complexes with, PRC2 [47], SAGA [48], and SET1 [49] providing well-studied paradigms. There is though, perhaps no greater variety of complexes housing a single enzymatic activity than the HDAC1/2 deacetylase complexes. HDAC1/2 are incorporated into six different families of multiprotein complexes (SIN3, NuRD, CoREST, MiDAC, MIER, and RERE) defined by multiple previous coIP/mass spectrometry studies [50–54]. Why the cell requires so many different vehicles for HDAC1/2 activity remains to be fully understood. While there have been extensive mapping studies, here we sought to address the possibility of a hierarchy among individual HDAC1/2 complexes. CoIP of HDAC1-Flag from HDAC1/2 DKO cells showed that there are three dominant HDAC1/2 complexes, NuRD (49%), CoREST (28%), and SIN3 (15%), constituting 92% of the total HDAC1 complexes in ESCs. The remaining complexes, MiDAC (3%), MIER (4%), and RERE (1%) make up a relatively minor cohort. Abundance does not entirely define importance of course, deletion of either of the MiDAC components, *Dnttip1* or *Mideas*, caused embryonic lethality in the mouse at e16.5 days [21]. However, KO studies involving components of the NuRD, SIN3A, and CoREST all produced early embryonic phenotypes prior to gastrulation, perhaps hinting at a greater importance at earlier time points [6]. Our experiments also provide insights into the relative composition of the different HDAC1/2 complexes. SIN3A appears to be 10-fold more abundant than SIN3B for instance (Fig. 1B). Similarly, the ratio of MBD3 versus MBD2 is 10:1, which may have implications for their distinct activities in the NuRD complex. These data also give an indication of each of the *core* complex components and those present in sub-stochiometric quantities, CHD4 versus CHD3 (a 325:1 ratio) in the NuRD complex, or CTBP2 versus CTBP1 (an 8:1 ratio) in the CoREST complex, being two of many examples (Fig. 1C). To gain an understanding of composition and abundance between cell types, we compared our data to the HDAC1 coIP reported by Vcelkova *et al.* [53] (shown in Supplementary Fig. S4). Consistent with our study, NuRD was also the most abundant complex by far in mouse embryo fibroblasts (MEFs) and HAP1 cells. However, the ratio of MBD3/MBD2 in MEFs is ∼1:1, compared with 10:1 in mouse ESCs. The MiDAC complex also appears to be similar in abundance to SIN3A and CoREST in MEFs (Supplementary Fig. S4). The abundance of proteins coIP experiments may reflect overall protein expression levels in the cell type being studied. To examine this, we compared the relative abundance of HDAC1/2 complex components in our coIP (Fig. 1) to protein copy numbers from the OpenCell resource [55]. The abundance of complex components in HEK293T cells (OpenCell) largely correlates with the amount of protein pulled-down in an HDAC1-Flag coIP (Supplementary Fig. S5), and again shows NuRD, CoREST, and SIN3A as the dominant complexes. Collectively, data from four different cell types support the assertion that NuRD, CoREST, and SIN3A are the three major HDAC1/2 complexes, and that the level of individual proteins in a complex may reflect overall protein abundance in the cell.

While there have been numerous HDAC1 mutations made previously, the bulk of these have focussed on the catalytic site of the enzyme [56–58]. We present here, the first systematic study of HDAC1 surface residues required to bind 15

separate interacting proteins from each of the 6 multiprotein complex families. Thirteen of these proteins utilize a combination of ELM2–SANT domains to bind to HDAC1, superficially at least, a cut-and-paste mechanism utilized by nature for interaction with HDAC1. Using a comparative analysis of HDAC1/MTA1 and HDAC1/MIDEAS structures [21, 24], we identified three separate regions utilized by these binary complexes (Fig. 2A). We hypothesized that loss of binding in any one of these regions would be insufficient to disrupt HDAC1 interaction since there would still be binding to the remaining two. To our surprise, we found that single (Y48E, K126E) and double (L161E/Y166E, Y333A/Y336A) mutations within each of these regions were capable of disrupting binding to all ELM2/SANT domain-containing proteins (Fig. 3 and Supplementary Fig. S1). Interestingly, Y333A/Y336A (in region 1), whose aromatic rings stack to support interactions with the SANT domain, abolished binding to all HDAC1-binders, including SIN3A/B. Y48 (in region 2) occupies a position on the surface that interacts with the dimerization domain of MTA1 (Fig. 2B, [24]). Mutation to glutamic acid (Y48E) caused loss of binding to all ELM2–SANT domain binders, but retention of binding SIN3A/B. An examination of these residues in other species from yeast to man showed almost complete conservation, with conservative changes (K126 to R and L161 to I) observed only in yeast (Supplementary Fig. S6). A model of the Rpd3 large complex from *Saccharomyces cerevisiae* (Rpd3L, equivalent to SIN3A) [13] showed that residues corresponding to Y48 (Y58) and E63 (E73) form part of a highly conserved surface and readily explain why both mutations are tolerated (Supplementary Fig. S7). Y58 is solvent exposed in both copies of Rpd3 and while it packs against other complex components (Dep1 and Pho23), it forms no significant contacts. E73 is both solvent exposed and far away from any other Rpd3L/SIN3A component. These data support our findings, highlight the relevance of the yeast models for the human counterpart, and demonstrate how well the SIN3A/HDAC complex is conserved despite over a billion years of evolution.

When we introduced HDAC1–Y48E into ESCs, we monitored *increased* binding to SIN3A/B complex components to the mutant (Fig. 3E), presumably because no other factors were competing for HDAC1 binding. Remarkably, HDAC1–Y48E was able to partially rescue the viability of HDAC1/2 DKO cells (~50% cell viability), suggesting that retention of the SIN3A/B complexes is sufficient for ESC viability (Fig. 3C). We identified a second more subtle mutation in region 3 (E63R) that has near WT deacetylase activity and ability to rescue DKO cells, and that discriminates between the different ELM–SANT complexes (Fig. 2B and Fig. 3D).

There is an assumption that most, if not all, HDAC1/2 complexes play a role in gene regulation. This has been demonstrated comprehensively for the three dominant complexes, NuRD, CoREST, and SIN3A, which are all recruited to DNA by a variety of transcription factors [6, 59]. The jury is still out in this regard for MiDAC and MIER, which have putative roles in mitosis [21, 51] and as a histone chaperone [60] respectively. Cells expressing HDAC1–Y48E retain only functional SIN3A and SIN3B complexes, which is sufficient to retain viability in ESCs, but results in global histone hyperacetylation and the dysregulation of over 3000 genes (Fig. 4A and B). The scale of the effect provides a potent example of the necessity for a full repertoire of ELM2–SANT domain containing complexes. HDAC1–E63R is the first mutation to discriminate between the binding of ELM2–SANT-dependent HDAC1-binding proteins (Fig. 3D). E63R bound MIER1-3 and RERE at the same level as WT while perturbing binding to MTA1-3, RCOR1/2, and MIDEAS (Fig. 3E). These data demonstrate for the first time that despite a common HDAC1 binding modality, the precise molecular interactions on the surface of the enzyme are distinct. In theory, at least, this might suggest that we could exploit differential binding to disrupt protein–protein interactions within each complex and thus generate a complex-specific HDAC inhibitor. In this study, we have defined critical residues on the surface of HDAC1 necessary for incorporation into a diverse group of multiprotein complexes and that against expectation, single point mutations are able to distinguish between the binding of even closely related ELM2/SANT-containing proteins. Consequently, different patterns of binding led to differential gene expression highlighting the distinct function of HDAC1/2 complexes in cells and development.

Acknowledgements

Thank you to members of the Cowley and Schwabe groups for critical comments and feedback on the data throughout the project. We thank Dr. Nicolas Sylvius and the NUCLEUS genomics facility for help with RNA extractions and quality checking of RNA/DNA. Plasmid constructs were generated by the PROTEX facility at the University of Leicester. This research used the ALICE High Performance Computing facility at the University of Leicester.

Author contributions: Ahmad Alshehri (Conceptualization [equal], Data curation [equal], Formal analysis [equal], Investigation [lead]), India M. Baker (Data curation [equal], Formal analysis [equal]), David M. English (Formal analysis [equal]), Louise Fairall (Formal analysis [equal]), Mark Collins (Formal analysis [equal], Investigation [equal], Methodology [equal]), John Schwabe (Conceptualization [equal], Formal analysis [equal]), and Shaun M. Cowley (Conceptualization [equal], Formal analysis [equal])

Supplementary data

Supplementary data is available at NAR online.

Conflicts of interest

There are no conflicts to declare.

Funding

The authors gratefully acknowledge funding from the following sources: Biotechnology and Biological Sciences Research Council (BBSRC) studentship from the Midlands Integrative Biosciences Training Partnership (MIBTP) [to I.M.B.]; Wellcome Trust Investigator Award [222493/Z/21/Z to J.W.R.S.]; MRC [MR/W00190X/1 to S.M.C.] and BBSRC [BB/P021689/1 to S.M.C.]; MRC [MR/X012220/1, MR/W00190X/1 to M.O.C.]. Funding to pay the Open Access publication charges for this article was provided by UKRI.

Data availability

The sequencing data underlying this study are available in GEO and can be accessed with the accession number

GSE278462. The mass spectrometry data have been deposited to the ProteomeXchange Consortium via the PRIDE partner repository with the dataset identifiers [PXD060154 (HDAC1 pulldowns) and PXD060158 (histone analysis)].

References

1. Barnes CE, English DM, Cowley SM. Acetylation & Co: an expanding repertoire of histone acylations regulates chromatin and transcription. *Essays Biochem* 2019;**63**:97–107.
2. Weinert BT, Narita T, Satpathy S *et al.* Time-resolved analysis reveals rapid dynamics and broad scope of the CBP/p300 acetylome. *Cell* 2018;**174**:231–244. https://doi.org/10.1016/j.cell.2018.04.033
3. Zheng Y, Thomas PM, Kelleher NL. Measurement of acetylation turnover at distinct lysines in human histones identifies long-lived acetylation sites. *Nat Commun* 2013;**4**:2203. https://doi.org/10.1038/ncomms3203
4. Millard CJ, Watson PJ, Fairall L *et al.* Targeting class I histone deacetylases in a "complex" environment. *Trends Pharmacol Sci* 2017;**38**:363–77. https://doi.org/10.1016/j.tips.2016.12.006
5. Asmamaw MD, He A, Zhang L-R *et al.* Histone deacetylase complexes: structure, regulation and function. *Biochim Biophys Acta* 2024;**1879**:189150. https://doi.org/10.1016/j.bbcan.2024.189150
6. Kelly RD, Cowley SM. The physiological roles of histone deacetylase (HDAC) 1 and 2: complex co-stars with multiple leading parts. *Biochem Soc Trans* 2013;**41**:741–9. https://doi.org/10.1042/BST20130010
7. Zhang Y, Xu M, Wang P *et al.* Structural basis for nucleosome binding and catalysis by the yeast Rpd3S/HDAC holoenzyme. *Cell Res* 2023;**33**:971–4. https://doi.org/10.1038/s41422-023-00884-2
8. Wang X, Wang Y, Liu S *et al.* Class I histone deacetylase complex: structure and functional correlates. *Proc Natl Acad Sci USA* 2023;**120**:e2307598120. https://doi.org/10.1073/pnas.2307598120
9. Wang C, Guo Z, Chu C *et al.* Two assembly modes for SIN3 histone deacetylase complexes. *Cell Discov* 2023;**9**:42. https://doi.org/10.1038/s41421-023-00539-x
10. Wan MS, Muhammad R, Koliopoulos MG *et al.* Mechanism of assembly, activation and lysine selection by the SIN3B histone deacetylase complex. *Nat Commun* 2023;**14**:2556. https://doi.org/10.1038/s41467-023-38276-0
11. Patel AB, Qing J, Tam KH *et al.* Cryo-EM structure of the *Saccharomyces cerevisiae* Rpd3L histone deacetylase complex. *Nat Commun* 2023;**14**:3061. https://doi.org/10.1038/s41467-023-38687-z
12. Li W, Cui H, Lu Z *et al.* Structure of histone deacetylase complex Rpd3S bound to nucleosome. *Nat Struct Mol Biol* 2023;**30**:1893–901.
13. Guo Z, Chu C, Lu Y *et al.* Structure of a SIN3–HDAC complex from budding yeast. *Nat Struct Mol Biol* 2023;**30**:753–60.
14. Guan H, Wang P, Zhang P *et al.* Diverse modes of H3K36me3-guided nucleosomal deacetylation by Rpd3S. *Nature* 2023;**620**:669–75. https://doi.org/10.1038/s41586-023-06349-1
15. Jelinic P, Pellegrino J, David G. A novel mammalian complex containing Sin3B mitigates histone acetylation and RNA polymerase II progression within transcribed loci. *Mol Cell Biol* 2011;**31**:54–62. https://doi.org/10.1128/MCB.00840-10
16. Cowley SM, Iritani BM, Mendrysa SM *et al.* The mSin3A chromatin-modifying complex is essential for embryogenesis and T-cell development. *Mol Cell Biol* 2005;**25**:6990–7004. https://doi.org/10.1128/MCB.25.16.6990-7004.2005
17. Dannenberg J-H, David G, Zhong S *et al.* mSin3A corepressor regulates diverse transcriptional networks governing normal and neoplastic growth and survival. *Genes Dev* 2005;**19**:6990–7004.
18. David G, Grandinetti KB, Finnerty PM *et al.* Specific requirement of the chromatin modifier mSin3B in cell cycle exit and cellular differentiation. *Proc Natl Acad Sci USA* 2008;**105**:4168–72. https://doi.org/10.1073/pnas.0710285105
19. Zhang T, Wei G, Millard CJ *et al.* A variant NuRD complex containing PWWP2A/B excludes MBD2/3 to regulate transcription at active genes. *Nat Commun* 2018;**9**:3798. https://doi.org/10.1038/s41467-018-06235-9
20. Hendrich B, Guy J, Ramsahoye B *et al.* Closely related proteins MBD2 and MBD3 play distinctive but interacting roles in mouse development. *Genes Dev* 2001;**15**:710–23.
21. Turnbull RE, Fairall L, Saleh A *et al.* The MiDAC histone deacetylase complex is essential for embryonic development and has a unique multivalent structure. *Nat Commun* 2020;**11**:3252. https://doi.org/10.1038/s41467-020-17078-8
22. Wang J, Hevi S, Kurash JK *et al.* The lysine demethylase LSD1 (KDM1) is required for maintenance of global DNA methylation. *Nat Genet* 2009;**41**:125–9. https://doi.org/10.1038/ng.268
23. Wang J, Scully K, Zhu X *et al.* Opposing LSD1 complexes function in developmental gene activation and repression programmes. *Nature* 2007;**446**:882–7. https://doi.org/10.1038/nature05671
24. Millard CJ, Watson PJ, Celardo I *et al.* Class I HDACs share a common mechanism of regulation by inositol phosphates. *Mol Cell* 2013;**51**:57–67. https://doi.org/10.1016/j.molcel.2013.05.020
25. Song Y, Dagil L, Fairall L *et al.* Mechanism of crosstalk between the LSD1 demethylase and HDAC1 deacetylase in the CoREST complex. *Cell Rep* 2020;**30**:2699–2711. https://doi.org/10.1016/j.celrep.2020.01.091
26. Jamaladdin S, Kelly RD, O'Regan L *et al.* Histone deacetylase (HDAC) 1 and 2 are essential for accurate cell division and the pluripotency of embryonic stem cells. *Proc Natl Acad Sci USA* 2014;**111**:9840–5. https://doi.org/10.1073/pnas.1321330111
27. Chandru A, Bate N, Vuister GW *et al.* Sin3A recruits Tet1 to the PAH1 domain via a highly conserved Sin3–interaction domain. *Sci Rep* 2018;**8**:14689. https://doi.org/10.1038/s41598-018-32942-w
28. Sidoli S, Kori Y, Lopes M *et al.* One minute analysis of 200 histone posttranslational modifications by direct injection mass spectrometry. *Genome Res* 2019;**29**:978–87. https://doi.org/10.1101/gr.247353.118
29. Baker IM, Smalley JP, Sabat KA *et al.* Comprehensive transcriptomic analysis of novel class I HDAC proteolysis targeting chimeras (PROTACs). *Biochemistry* 2023;**62**:645–56. https://doi.org/10.1021/acs.biochem.2c00288
30. Alexa A, Rahnenführer J. Gene set enrichment analysis with topGO. *Bioconductor Improv* 2009;**27**:1–26.
31. Schwanhäusser B, Busse D, Li N *et al.* Global quantification of mammalian gene expression control. *Nature* 2011;**473**:337–42. https://doi.org/10.1038/nature10098
32. Millard CJ, Fairall L, Ragan TJ *et al.* The topology of chromatin-binding domains in the NuRD deacetylase complex. *Nucleic Acids Res* 2020;**48**:12972–82. https://doi.org/10.1093/nar/gkaa1121
33. Cao R, Zhang Y. SUZ12 is required for both the histone methyltransferase activity and the silencing function of the EED-EZH2 complex. *Mol Cell* 2004;**15**:57–67. https://doi.org/10.1016/j.molcel.2004.06.020
34. Kuzmichev A, Nishioka K, Erdjument-Bromage H *et al.* Histone methyltransferase activity associated with a human multiprotein complex containing the Enhancer of Zeste protein. *Genes Dev* 2002;**16**:2893–905.
35. Laherty CD, Yang WM, Sun JM *et al.* Histone deacetylases associated with the mSin3 corepressor mediate mad transcriptional repression. *Cell* 1997;**89**:349–56. https://doi.org/10.1016/S0092-8674(00)80215-9
36. Zhang Y, Iratni R, Erdjument-Bromage H *et al.* Histone deacetylases and SAP18, a novel polypeptide, are components of a human Sin3 complex. *Cell* 1997;**89**:357–64. https://doi.org/10.1016/S0092-8674(00)80216-0
37. Zhang Y, LeRoy G, Seelig HP *et al.* The dermatomyositis-specific autoantigen Mi2 is a component of a complex containing histone

deacetylase and nucleosome remodeling activities. *Cell* 1998;**95**:279–89. https://doi.org/10.1016/S0092-8674(00)81758-4
38. Huttlin EL, Bruckner RJ, Navarrete-Perea J *et al.* Dual proteome-scale networks reveal cell-specific remodeling of the human interactome. *Cell* 2021;**184**:3022–3040. https://doi.org/10.1016/j.cell.2021.04.011
39. van den Berg DL, Snoek T, Mullin NP *et al.* An Oct4-centered protein interaction network in embryonic stem cells. *Cell Stem Cell* 2010;**6**:369–81. https://doi.org/10.1016/j.stem.2010.02.014
40. Yang J, Chai L, Fowles TC *et al.* Genome-wide analysis reveals Sall4 to be a major regulator of pluripotency in murine-embryonic stem cells. *Proc Natl Acad Sci USA* 2008;**105**:19756–61. https://doi.org/10.1073/pnas.0809321105
41. Williams K, Christensen J, Pedersen MT *et al.* TET1 and hydroxymethylcytosine in transcription and DNA methylation fidelity. *Nature* 2011;**473**:343–8. https://doi.org/10.1038/nature10066
42. Yang X, Zhang F, Kudlow JE. Recruitment of O-GlcNAc transferase to promoters by corepressor mSin3A: coupling protein O-GlcNAcylation to transcriptional repression. *Cell* 2002;**110**:69–80. https://doi.org/10.1016/S0092-8674(02)00810-3
43. Watson PJ, Millard CJ, Riley AM *et al.* Insights into the activation mechanism of class I HDAC complexes by inositol phosphates. *Nat Commun* 2016;**7**:11262. https://doi.org/10.1038/ncomms11262
44. Kim YJ, Greer CB, Cecchini KR *et al.* HDAC inhibitors induce transcriptional repression of high copy number genes in breast cancer through elongation blockade. *Oncogene* 2013;**32**:2828–35. https://doi.org/10.1038/onc.2013.32
45. Leitch HG, McEwen KR, Turp A *et al.* Naive pluripotency is associated with global DNA hypomethylation. *Nat Struct Mol Biol* 2013;**20**:311–6.
46. Abramson J, Adler J, Dunger J *et al.* Accurate structure prediction of biomolecular interactions with AlphaFold 3. *Nature* 2024;**630**:493–500.
47. van Mierlo G, Veenstra GJC, Vermeulen M *et al.* The complexity of PRC2 subcomplexes. *Trends Cell Biol* 2019;**29**:660–71. https://doi.org/10.1016/j.tcb.2019.05.004
48. Grant PA, Winston F, Berger SL. The biochemical and genetic discovery of the SAGA complex. *Biochim Biophys Acta* 2021;**1864**:194669. https://doi.org/10.1016/j.bbagrm.2020.194669
49. Jiang H. The complex activities of the SET1/MLL complex core subunits in development and disease. *Biochim Biophys Acta* 2020;**1863**:194560. https://doi.org/10.1016/j.bbagrm.2020.194560
50. Banks CA, Miah S, Adams MK *et al.* Differential HDAC1/2 network analysis reveals a role for prefoldin/CCT in HDAC1/2 complex assembly. *Sci Rep* 2018;**8**:13712. https://doi.org/10.1038/s41598-018-32009-w
51. Bantscheff M, Hopf C, Savitski MM *et al.* Chemoproteomics profiling of HDAC inhibitors reveals selective targeting of HDAC complexes. *Nat Biotechnol* 2011;**29**:255–65. https://doi.org/10.1038/nbt.1759
52. Joshi P, Greco TM, Guise AJ *et al.* The functional interactome landscape of the human histone deacetylase family. *Mol Syst Biol* 2013;**9**:672. https://doi.org/10.1038/msb.2013.26
53. Vcelkova T, Reiter W, Zylka M *et al.* GSE1 links the HDAC1/CoREST co-repressor complex to DNA damage. *Nucleic Acids Res* 2023;**51**:11748–69. https://doi.org/10.1093/nar/gkad911
54. Zhu C, Stolz V, Simonovic N *et al.* Targeting the catalytic activity of HDAC1 in T cells protects against experimental autoimmune encephalomyelitis. bioRxiv, https://www.biorxiv.org/content/10.1101/2023.04.14.536700v1, 14 April 2023, preprint: not peer reviewed.
55. Cho NH, Cheveralls KC, Brunner AD *et al.* OpenCell: endogenous tagging for the cartography of human cellular organization. *Science* 2022;**375**:eabi6983. https://doi.org/10.1126/science.abi6983
56. Hassig CA, Tong JK, Fleischer TC *et al.* A role for histone deacetylase activity in HDAC1-mediated transcriptional repression. *Proc Natl Acad Sci USA* 1998;**95**:3519–24. https://doi.org/10.1073/pnas.95.7.3519
57. Hess L, Moos V, Lauber AA *et al.* A toolbox for class I HDACs reveals isoform specific roles in gene regulation and protein acetylation. *PLoS Genet* 2022;**18**:e1010376. https://doi.org/10.1371/journal.pgen.1010376
58. Weerasinghe SVW, Estiu G, Wiest O *et al.* Residues in the 11 Å channel of histone deacetylase 1 promote catalytic activity: implications for designing isoform-selective histone deacetylase inhibitors. *J Med Chem* 2008;**51**:5542–51. https://doi.org/10.1021/jm800081j
59. Moser MA, Hagelkruys A, Seiser C. Transcription and beyond: the role of mammalian class I lysine deacetylases. *Chromosoma* 2014;**123**:67–78. https://doi.org/10.1007/s00412-013-0441-x
60. Wang S, Fairall L, Pham TK *et al.* A potential histone-chaperone activity for the MIER1 histone deacetylase complex. *Nucleic Acids Res* 2023;**51**:6006–19. https://doi.org/10.1093/nar/gkad294

Received: March 25, 2025. **Revised:** July 24, 2025. **Accepted:** August 20, 2025